Hairus_Abdullah_et_al._Chemistry_Select_2021.pdf

by

Submission date: 08-Nov-2021 03:07PM (UTC+0700)
Submission ID: 1696491655
File name: Hairus_Abdullah_et_al._Chemistry_Select_2021.pdf (3.66M)
Word count: 5693
Character count: 28764

Catalysis

Visible-Light Driven Ni-Incorporated CdS Photocatalytic Activities for Azo-Bond Cleavages with Hydrogenation Reaction

Hairus Abdullah,[a] Rikson Siburian,*[b] Subur P. Pasaribu,[c] and Aman S. Panggabean[c]

Ni-incorporated CdS (Ni-CdS) photocatalysts with different amounts of Ni dopant have been synthesized, characterized, and examined toward azo-bond cleavages in visible-light illuminated conditions. The optimum performance was achieved with a relatively low amount of Ni dopant (2% atomic mass). The azo bonds of azobenzene (AB) and methyl orange (MO) compounds were hydrogenated with the in-situ generated hydrogen on Ni-CdS catalyst surfaces. The hydrogen evolution reaction was proved and measured with GC measurement during the photocatalytic session with an incandescent halogen lamp. Furthermore, the experimental data of UV-vis spectra analyses suggested the formation of aniline or sodium sulfanilate and p-aminodimethylaniline with the emerged peaks at ~240 nm, indicating azo-bond has been cleaved in AB or MO compounds, respectively. The catalytic performances of 2% Ni-CdS are also supported with electrical and photoresponse analyses. To demonstrate the possibility of industrial application, Ni-CdS catalyst stability is also tested for several runs in reusability experiments and examined with cyclic voltammetry for 100 cycles without any significant degradation. The cleavage mechanisms of azo bonds in AB and MO compounds were discussed and proposed in this work.

1. Introduction

The carbon-based energy source has posed severe problems to our environment due to the emitted greenhouse gases. In recent decades, the exploration of renewable energy sources has been widely done by focusing on visible-light harnessing materials.[1] The works on visible-light active materials are favorable since most of the solar light spectrum contains about 44% visible light and only ~4% UV light was available in the spectrum.[2] One of the promising energy sources is utilizing sustainable hydrogen gas as an energy carrier harvested from solar light. One of the promising methods to produce hydrogen gas is visible-light photocatalysis under solar light illumination. The generation of hydrogen gas with different concepts such as heterojunction formation, solid solution, dye-sensitized mechanism, and localized surface plasmonic resonance (LSPR) have been strived to obtain a highly efficient process.[3] As the mechanism is initiated with adsorbed hydrogen ions on catalyst surfaces,[4] the in-situ generated hydrogen can be utilized for a further hydrogenation reaction in mild conditions without using additional reducing agents. Therefore, the visible-light photocatalytic hydrogenation method with a mild condition is auspicious and worth exploring for future industrial applications.

A green chemical conversion utilizing the photocatalysis method is an essential application for industries to promote environmentally benign chemical conversion with a crucial fundamental of chemistry.[3h] The basic photocatalytic reaction is oxidation and reduction with photo-generated hole and electron, respectively. It has been avidly demonstrated with TiO_2 semiconductor with photo-generated $OH^{\bullet}$ radical to oxidize many toxic organics.[5] In the other case, the photocatalytic reduction is also useful for chemical conversions, such as converting toxic 4-nitrophenol (4-NP) to a useful 4-aminophenol (4-AP) chemical without using reducing agents in a mild condition.[3h,6] Most of the works for the 4-NP-to-4-AP conversion, the common $NaBH_4$ or NH_4HCO_2 as hydrogen sources are utilized to accelerate the reduction reaction.[1,19] The advantages of photocatalysis method are the cleanliness of reaction and safety due to the self-generated proton for chemical conversion. Therefore, the photocatalytic method is promising and encouraging to be further explored to expand its environmentally friendly application.[6a,7]

As aniline is important intermediates for dyestuffs, polyurethane, and pharmaceuticals in industries,[8] it is economically viable to work on chemical conversion to synthesize aniline in a mild condition. Nowadays, the synthesis of aniline involves two main steps. The first step is to nitrate benzene with concentrated nitric acid and sulfuric acid to produce nitrobenzene (NB) at ~60 °C, followed by a hydrogenation reaction at ~300 °C.[9] Other synthesis procedures of aniline from NB can also be done at 90–125 °C under high pressure of hydrogen[10] or H_2 pressure at 3 MPa in ionic liquid[11] or at room temper-

[a] Dr. H. Abdullah
Department of Industrial Engineering, Universitas Prima Indonesia, Medan, Indonesia
[b] Dr. R. Siburian
Department of Chemistry, Faculty of Mathematics and Natural Sciences, Universitas Sumatera Utara, Medan-20155, Indonesia
E-mail: rikson@usu.ac.id
[c] Dr. S. P. Pasaribu, Prof. A. S. Panggabean
Department of Chemistry, Faculty of Mathematics and Natural Sciences, Mulawarman University, Samarinda-75123, Indonesia

Supporting information for this article is available on the WWW under https://doi.org/10.1002/slct.202004214

ature with electrocatalysis.[12] On the other way, NB also can be chemically converted to aniline over Bi_2MoO_6 with ammonium oxalate as a reducing agent or over g-C_3N_4 with hydrazine in 80 °C water.[11,13] Furthermore, the 4-NP-to-4-AP conversion in a mild condition also needs a strong reducing agent to provide hydrogen ions.

As visible-light photocatalytic process needs generated electron and hole which occurred in an illuminated light with a wavelength more than 400 nm, materials selection and design play an important role to harness most of the solar spectrum. The famous photocatalytic material of TiO_2 has demonstrated its capability to evolve hydrogen in many works since its first work in 1972.[14] However, wide bandgap and utilization of noble metal of Pt are the main obstacles in its development. Therefore, many works endeavor to modify TiO_2 with visible-light active materials such as Cu_2O, Ag_2O, $BiVO_4$, and Fe_3O_4.[1i,15] Although some works have successfully modified TiO_2 for visible-light photocatalysis, Pt or Au as noble metal are still needed as a co-catalyst during the photoreactions.[3d,15a,16] Another critical concept to enhance catalysts' activities is introducing a certain dopant into the catalyst lattice to induce defects that could trap photo carriers that enhance their lifetime.[1h,17] One of the famous visible light active materials is CdS with a suitable bandgap of 2.4 eV.[18] The modification of CdS materials has been done with ZnSe, Pt, CuS, MnS, etc. to enhance the efficiency reaction.[18–19] It is noticed that the incorporation of Ni into CdS enhances the properties for photovoltaic parameters,[20] high voltage applications,[21] and optical applications.[22] However, the application for photo-catalytic hydrogenation for the chemical conversion is not yet done. The present work is to study the effects of Ni on properties of CdS related to the capabilities to cleave the azo bond in an aqueous solution.

To address the abovementioned issues, Ni-doped CdS was prepared by a simple method at relatively low temperatures. The as-prepared yellowish powders of Ni-CdS are tested toward azobenzene and methyl orange to cleave the azo bonds in the compounds. The experimental data of UV-vis spectra indicated the cleavages of azo bonds were done in a relatively short reaction time of 2 h in the presence of 2% Ni-CdS in ethanol solution. Finally, the azo bond cleavage mechanism on the Ni-CdS catalyst is elucidated and proposed with supported data.

2. Results and discussions

2.1. X-ray diffraction patterns

To identify the phases of as-prepared catalyst powders, X-ray diffractometer analysis was carried out for Ni-CdS with different Ni contents. Figure 1 shows the diffraction patterns of Ni-CdS with 0, 2, 5, and 10% Ni dopant and JCPDS file (#77-2306) of hexagonal CdS as a standard pattern. All the major peaks of Ni-CdS were consistent with those of hexagonal CdS. A peak shift at (110) to a higher angle was observable as Ni contents increased, indicating the Ni dopant had been incorporated into CdS lattices to induce the lattice parameter at (110) smaller. The peak at (110) was magnified to quickly notice the peak shift about 0.1–0.3° to a higher angle depended on dopant contents as indicated in Figure 1. The peak shift was related to the smaller size of Ni atom (135 pm) occupied Cd site (atomic size of Cd is ~155 pm), which imposed a shrinkage in the lattice.[23] However, the peak at ~45° became a little broader after doping with 5% and 10% Ni, indicating a small amount of Ni metal was precipitated. The peak position at ~45° for Ni metal was confirmed with PDF file #04-0850 which indicated Ni metal possessed a peak at ~45° with the highest intensity. The small peak of Ni was not obviously noticeable since it was

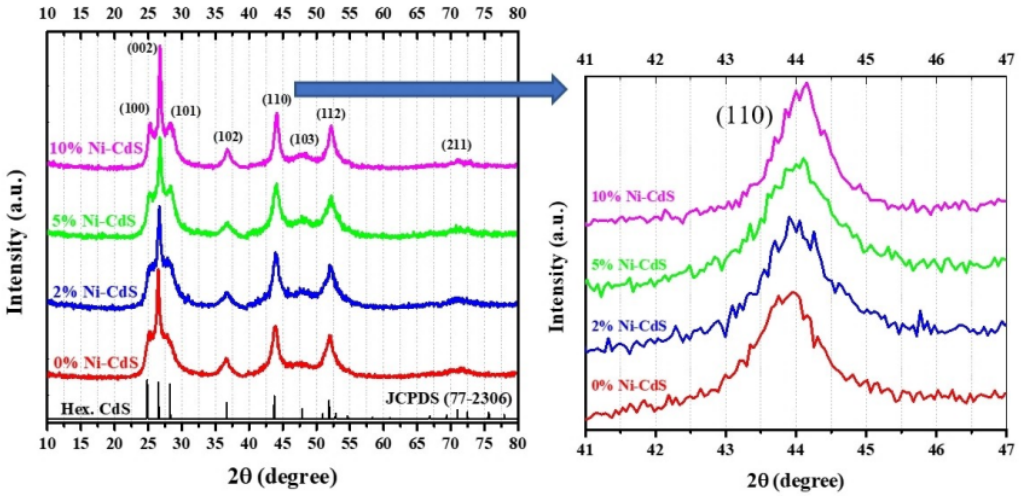

Figure 1. XRD patterns of different Ni-incorporated CdS catalysts indicated a peak shift at (110) and JCPSDS #77-2306 as a standard pattern of hexagonal CdS.

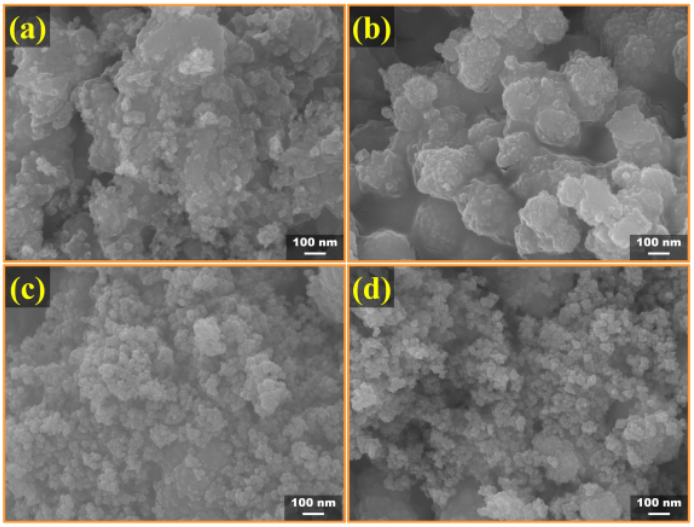

Figure 2. SEM images of Ni-CdS with (a) 0%, (b) 2%, (c) 5%, and (d) 10% Ni dopant.

overlapped with the CdS peak at (103). Based on Scherrer equation, the crystalline sizes of Ni-CdS particles were ~11.8, 16.6, 10.1, and 11.3 nm for 0, 2, 5, and 10% Ni dopants, respectively. XRD analysis indicated Ni atoms had been successfully doped into CdS lattices to form single-phase Ni-doped CdS catalyst.

Table 1. EDS analysis of Ni-CdS catalysts.

Samples	Elements (atomic %) Cd	S	Ni
0% Ni-CdS	52.56±0.59	47.44±1.01	0±0.05
2% Ni-CdS	52.24±1.36	47.39±1.84	0.37±0.77
5% Ni-CdS	51.27±0.74	47.54±0.35	1.19±0.52
10% Ni-CdS	50.05±0.41	47.91±0.87	2.03±0.64

2.2. Scanning electron microscopy (SEM) and electron dispersive spectroscopy (EDS) analyses

The microstructure and morphology as well as EDS analyses of Ni-CdS catalysts were probed with a scanning electron microscope. Figure 2 indicates the SEM images of Ni-CdS with different amounts of Ni dopant. It was observed that the particle sizes of catalysts were very tiny, which induced the aggregation to form a considerable size of the particle. There was no significant difference in the nanoparticle (NP) morphology between CdS NPs and without Ni dopant. The small size of particle was also confirmed with the result of Scherrer's calculation in XRD analysis. As observed in the SEM images, the particle size was around 10–20 nm, which was propitious to catalytic activities.[1g,22] To confirm the actual content of each element in the Ni-CdS catalyst, EDS analysis was carried out during the SEM measurement. Table 1 shows the amounts of each element in Ni-CdS catalysts with different Ni contents. The percentages of Cd and S were close to the stoichiometric ratio and the amounts of Ni in CdS catalyst increased as the amount of Ni dopant increased. However, the amount of Ni to incorporate into CdS lattices was relatively low might be due to the low-temperature synthesis. As the significant composition in catalysts contained Cd and S with almost stoichiometric ratio, it also confirmed the formation of CdS single phase, which is consistent with XRD analysis. Furthermore, the Ni contents determined by ICP analysis were found to be 0, 69±21, 173±10, 209±14 μg/mL for 0, 2, 5, and 10% Ni-CdS, respectively as shown in Figure S2.This result also showed a good correlation with the EDS data in Table 1.

2.3. Diffuse reflectance spectroscopy (DRS) analysis

DRS analysis is one of the most crucial characterizations to probe the optical properties of photocatalyst materials. The analysis was conducted for all as-prepared Ni-CdS catalysts with different contents of Ni dopant. Figure 3 indicates the light absorbances of Ni-CdS catalysts and the determination of bandgap energy with a Tauc plot. The light absorbance spectra revealed the main activities of Ni-CdS catalysts were induced by photons with a wavelength between 300–550 nm, which implies the catalysts could be activated with UV–A and visible light illumination. As compared with solar spectrum,[1 5d,24] these catalysts might absorb more than 50% light spectrum under solar light illumination. The light absorbance profiles of Ni-CdS catalysts were not significantly changed with different amounts of Ni, except the one with 2% Ni exhibited the light absorbance in the UV region was decreased. All the catalysts showed the same absorbance edges, indicating the incorpo-

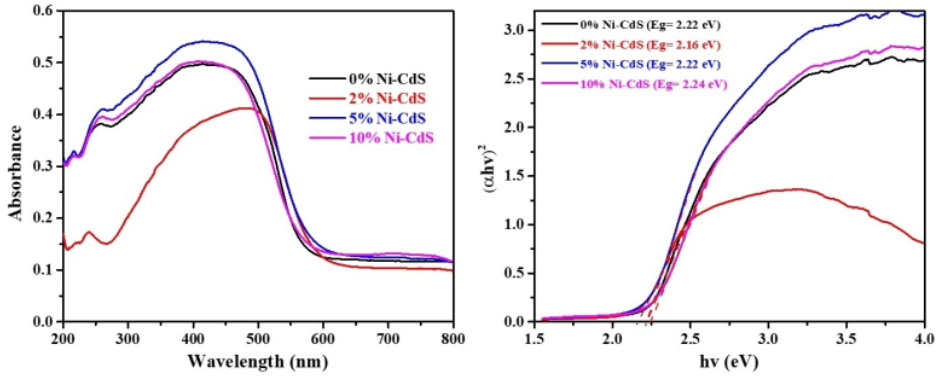

Figure 3. Diffuse reflectance spectra (right) and Tauc plots (left) of Ni-CdS catalysts with different Ni dopant amounts.

ration of Ni did not obviously alter the bandgap of catalyst. To determine the bandgap values of catalysts, a Tauc plot was derived based on the DRS spectra. CdS materials possessed a direct bandgap which could be calculated based on the fitting as shown in Figure 3. The bandgap values of 0, 2, 5, and 10% Ni-CdS were 2.22, 2.16, 2.22, and 2.24 eV, respectively which did not differ too much as indicated with the same absorbance edges.

2.4. Transient photocurrent (TPC) analysis

TPC analysis was conducted to probe the capabilities of catalysts to respond to the incident light with induced current during the light illumination. As photon energy excited the electron from valence band to conduction band, the electron would flow from working electrode to counter electrode so that the amounts of electrical charges could be observed during the measurement. TPC analysis was done with an electrochemical station utilizing catalyst-modified glassy carbon electrode (GCE), Ag/AgCl/sat KCl, and Pt as working, reference, and counter electrodes, respectively and 1 M KCl was used as electrolyte during the measurement. To deposit the catalyst powder on GCE, 10 mg catalyst was dispersed in Nafion solution and the solution was wisely dropped and dried on GCE. 10 W white LED lamp was used as a light source in the analysis. To show the response of catalyst with incident light, the lighting was alternately switched on and off with a frequency of 25 mHz during the measurement. Figure 4 indicates the transient photocurrent spectra of Ni-CdS with different Ni contents. The highest induced current was achieved at 2 μA/cm² with 2% Ni-CdS-modified GCE which was significantly different from other Ni-CdS catalysts due to the Ni

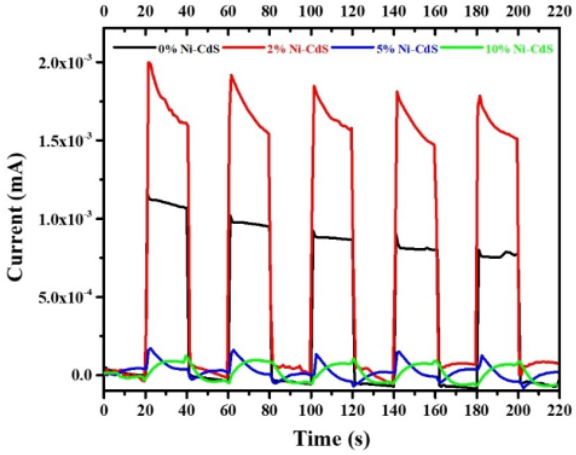

Figure 4. Transient photocurrent spectra of Ni-CdS with different Ni dopant contents with a light-on/off-illumination frequency of 25 mHz.

metal was precipitated at higher percentages. The higher photocurrent with 2% Ni-CdS indicated the photoinduced electrical charges were effectively transferred from catalyst to counter electrode, implying a good indication for photocatalytic activities related to facile charge transport.[3g]

2.5. Electrochemical impedance spectroscopy (EIS) analysis

Another crucial analysis of EIS was also carried out in 1 M KCl electrolyte to support the TPC analysis results. Three-electrode measurement as done in TPC analysis was used in EIS analysis with a potential at −1 V and frequencies from 50 kHz–0.1 Hz. The analysis is to probe the electrical property of catalysts related to the charge transfer behavior during the electrochemical measurement. Figure 5 reveals the Nyquist plots of Ni-CdS catalysts with different amounts of Ni dopant. The spectra of EIS were fitted with an equivalent Randles circuit to determine the charge transfer resistances of catalysts. The smaller semicircle spectra indicated lower charge resistance, which is propitious to enhance photocatalytic activities. As indicated with Nyquist plots, the charge transfer resistivities of 0, 2, 5, and 10% Ni-CdS were 910, 745, 1325, and 3090 Ω, respectively. It was found that 2% Ni-CdS exhibited the lowest charge transfer resistivity as compared to others due to the Ni precipitation at higher amounts, which was consistent with TPC analysis. Based on the TPC and EIS analysis, 2% Ni-CdS might be excellent for photocatalytic activities.

2.6. Photocatalytic azo bond cleavages of AB and MO

The photocatalytic activities of Ni-CdS catalysts were examined toward performances of azo bond cracking in AB and MO compounds. The photocatalytic cleavages of azo bonds were carried out for all as-prepared Ni-CdS catalysts with different Ni contents. Figure 6 and 7 indicate the UV-vis spectra of AB and MO solution after photocatalytic reaction with different reaction times. In the case of UV-vis spectra of AB, the peak located at ~320 nm was attributed to cis-AB as the trans-AB was quickly changed to cis-AB under light illumination. Figure 6a, b, c, and d show the UV-vis spectra of reaction solution containing ten ppm AB in the presences of 0, 2, 5, and 10% Ni-CdS catalysts, respectively. Before doping with Ni, CdS catalyst could not effectively break the azo bond as indicated with the peak at ~320 nm, which was still appeared after 120 min photocatalytic reaction. However, when Ni was incorporated into CdS, the cis-AB peak was totally disappeared after 120 min reaction and the other peaks at 239 nm attributed to aniline were gradually shown up.[4a,d] The best photocatalytic cleavage of azo bond was achieved with 2% Ni-CdS which was indicated with the rapid degradation of cis-AB peak at ~320 nm and the gradually emerged peak at 239 nm for aniline, indicating the cis-AB was broken to form aniline as the azo bond was cleaved. To show the cleavage of azo-bond in MO compound, the same experimental procedure was used and the UV-vis spectroscopy results were shown in Figure 7a, b, c, dan d, which were related with 0, 2, 5, and 10% Ni-CdS dispersed solution after the photocatalytic reaction, respectively. The prominent peak of MO at ~462 nm was decreased as the other peak at 244 nm increased. The emerged peak at 244 nm was contributed to the products of sodium sulfanilate and p-aminodimethylaniline as the azo bond in the MO structure was cleaved.[25] Both of the products contained an amine group which induced an overlapping peak at 244 nm. As the MO was reduced, the solution color was also changed to colorless, as shown in Figure 7b. The result in Figure 7 indicated 2% Ni- CdS catalyst degraded the central peak of MO very fast and induced a new peak at

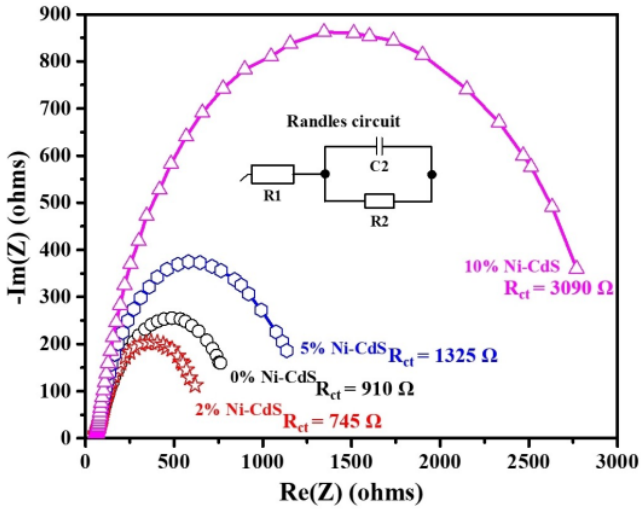

Figure 5. Nyquist plots of Ni-CdS with different amounts of Ni dopant with equivalent Randles circuit fitted spectra.

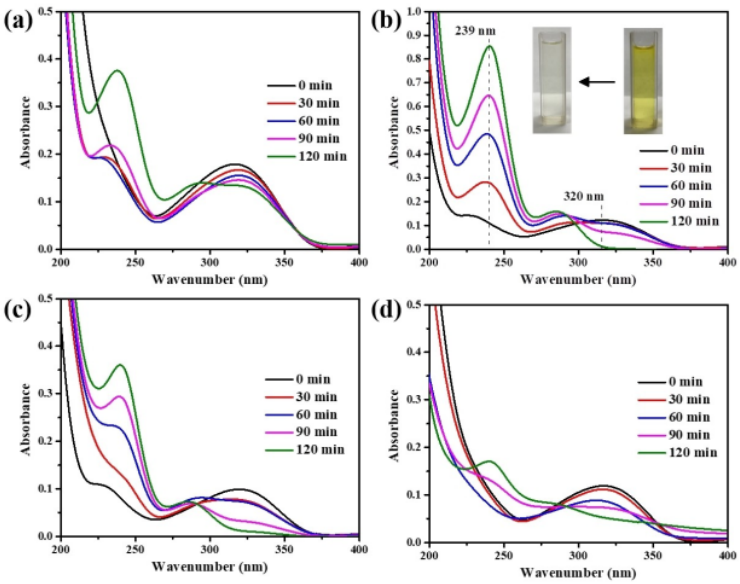

Figure 6. UV-vis spectra of 10 ppm AB solution with different reaction times in the presences of (a) 0%, (b) 2%, (c) 5%, and (d) 10% Ni-CdS catalysts during visible-light photocatalytic reaction.

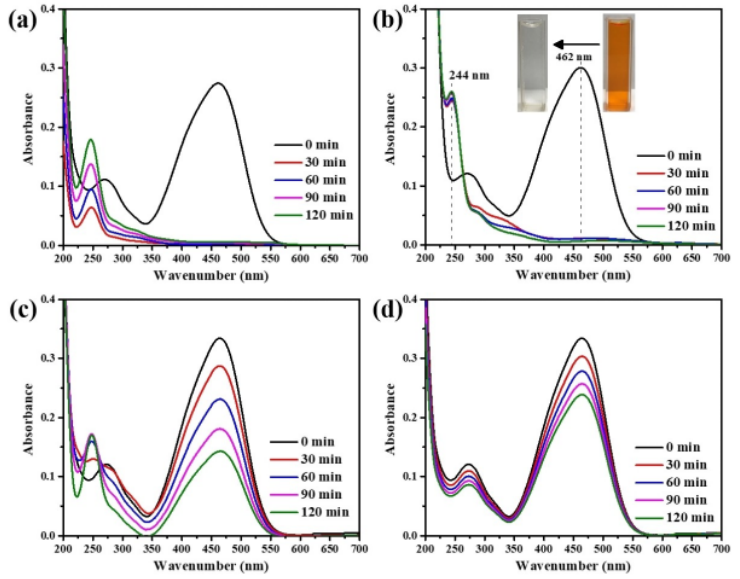

Figure 7. UV-vis spectra of 20 ppm MO solution with different reaction times in the presences of (a) 0%, (b) 2%, (c) 5%, and (d) 10% Ni-CdS catalysts during visible-light photocatalytic reaction.

244 nm for the reduction products. Although the CdS without Ni degraded the prominent peak of MO very fast, however, the intensity of aniline peak at ~240 nm was not as high as CdS with 2% Ni dopant, indicating the azo bond cleavage was more effective with 2% Ni-CdS. The other Ni-CdS catalysts with 0, 5, and 10% Ni dopant could not degrade the MO peak in

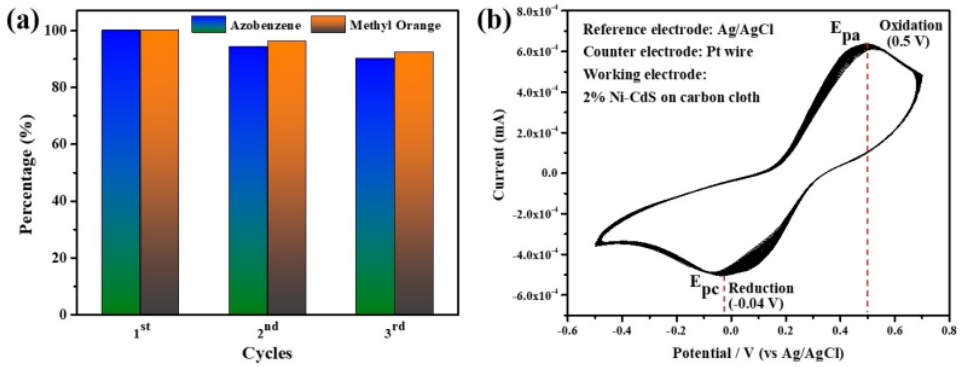

Figure 8. (a) Reusability of 2% Ni-CdS catalyst in cleaving azo group in AB and MO compounds for three consecutive runs and (b) cyclic voltammogram of 2% Ni-CdS catalyst in 1 M KCl electrolyte with Fe^{2+} and Fe^{3+} as active species for oxidation and reduction reaction.

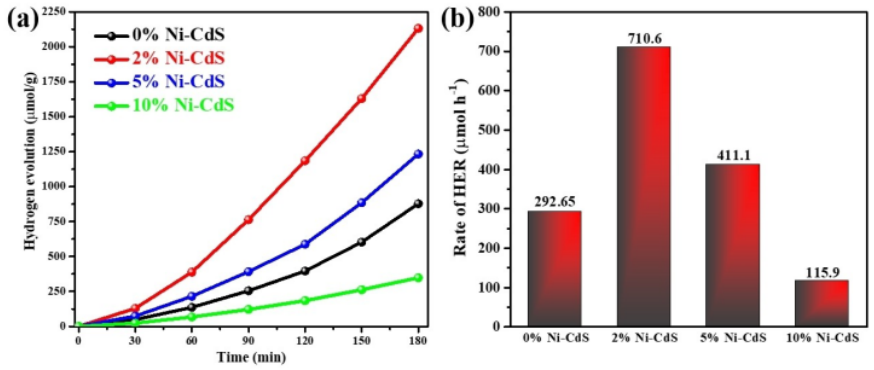

Figure 9. (a) Photocatalytic hydrogen evolution reactions of Ni-CdS with different Ni contents and (b) their total amounts of evolved hydrogen after 5-h reactions.

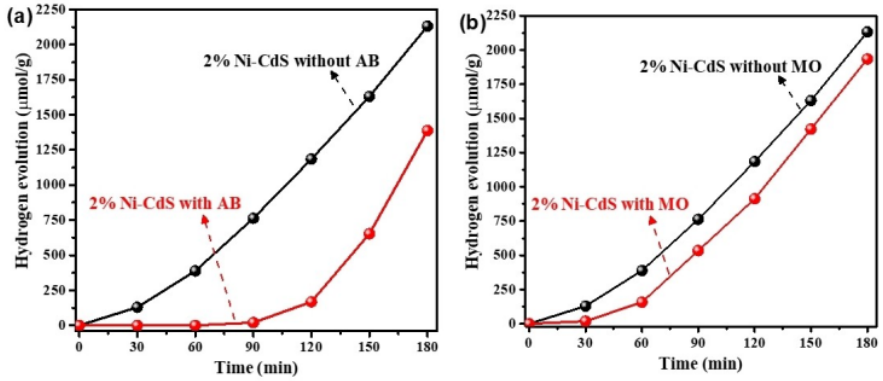

Figure 10. Photocatalytic hydrogen evolution amounts of 2% Ni-CdS with and without (a) AB and (b) MO in 10% ethanol solution, indicating the in situ generated hydrogen was utilized for the azo bond cleavages.

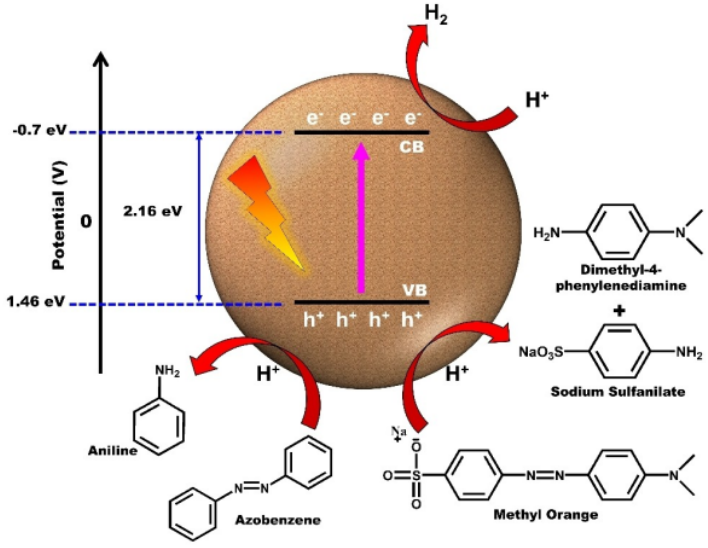

Figure 11. Photocatalytic azo bond cleavages of AB and MO compounds in the presence of 2% Ni-CdS catalyst in a visible-light illuminated condition.

120 min, implying worse catalytic activities to cleave the azo bonds. The experimental results also revealed that the TPC and EIS analyses were consistent with the photocatalytic activities of 2% Ni-CdS catalyst with a relatively higher photocurrent and lower charge transfer resistivity. Based on the proofs that the peak degradations at 320 nm for cis-AB and at 462 nm for MO and the emergences of new peaks at 239 nm for aniline and at 244 nm for the products of MO reduction,[4a,d,25b] the photocatalytic reactions had successfully cleaved the azo bonds in AB and MO compounds in the presences of Ni-CdS catalysts.

2.7. Reusability

As the excellent performance of photocatalytic azo bond cleavage was achieved with a 2% Ni-CdS catalyst, the catalyst's stability was also needed to test with a reusability experiment and cyclic voltammetry (CV) measurement. To experimentally test the long-term application for photocatalytic azo bond cleavages, the catalyst was consecutively tested for three runs to reduce AB and MO in a separate experiment. The results shown in Figure 8a indicated an insignificant degradation of catalyst to cleave the azo bonds in AB and MO compounds. The small degradation of performances might be due to the coverage of reduction products of aniline, sodium sulfanilate, and p-aminodimethylaniline on catalyst surfaces. However, the efficiencies of azo bond cleavages still achieved ~90% for both AB and MO compounds, indicating good stability of Ni-CdS catalyst, which is promising for real application in chemical industries. To further show the stability of the Ni-CdS catalyst, CV measurement was selected to run for 100 cycles in 1 M KCl solution with Fe^{2+} and Fe^{3+} as active redox species. The measurement was carried out with three-electrode measurement with catalyst-modified carbon cloth, Ag/AgCl/KCl, and Pt wire as working, reference, and counter electrodes, respectively. The anodic and cathodic peaks were located at 0.5 and −0.04 V, respectively, related to oxidation and reduction peaks of Fe^{2+} and Fe^{3+}. The CV measurement indicated the same redox process should be continuously occurred to provide hydrogen ions as a reducing agent to cleave azo bonds during the photocatalytic reaction. As the CV spectra in Figure 8b had shown a stable profile for oxidation and reduction of Fe ions, 2% Ni-CdS catalyst was suggested to be used for long-term application. The mechanisms of reduction and oxidation of ferri-ferrocyanide redox couple were believed to occur following Eqs (1) and (2).[26]

$$\text{Reduction}: [Fe(CN)_6]^{3-} + e^- \rightarrow [Fe(CN)_6]^{4-} E^\circ = -0.04\,V \ (\text{vs Ag/AgCl}) \quad (1)$$

$$\text{Oxidation}: [Fe(CN)_6]^{4-} \rightarrow [Fe(CN)_6]^{3-} + e^- E^\circ = 0.5\,V \ (\text{vs Ag/AgCl}) \quad (2)$$

2.8. Photocatalytic mechanisms of azo bond cleavages

To elucidate the photocatalytic azo bond cleavages, hydrogen evolution reaction in ethanol solution with and without AB or MO was carried out to show the amount of evolved hydrogen during the photocatalytic reaction. All of the as-prepared catalysts were tested for photocatalytic HER. The results indicated that CdS with 2% Ni dopant achieved the highest hydrogen evolution rate of 710 μmol/h as shown in Figure 9 since the doping with 2% Ni induced the highest photo-

response lowest resistivity to CdS catalyst as confirmed with TPC and EIS analyses. The evolved hydrogen amounts from the solutions without AB or MO were higher than those with AB or MO, indicating the in situ generated hydrogen was utilized for the azo bond cleavages, as shown in Figure 10. The photocatalytic azo bond cleavages were initiated with photoexcitation to generate electron and hole in the conduction band and valence band, respectively, as shown in Eq. (3). The photogenerated hole would oxidize water and ethanol to form H^+ as indicated in Eqs. (4) and (5), respectively. The hydrogen ions would be further reduced by the photo-generated electron to hydrogen gas as shown in Eq. (6) if AB or MO compounds were not available in the reaction solution. In the presence of AB or MO, the adsorbed H^+ on catalyst surfaces could be utilized to hydrogenate the azo bonds to form aniline or sodium sulfanilate and p-aminodimethylaniline, respectively, as indicated in Eqs. (7) and (8).

$$2\,\%\ Ni-CdS \rightarrow e^- + h^+ \quad (3)$$

$$H_2O + h^+ \rightarrow H^+ + OH^- \quad (4)$$

$$C_2H_5OH + h^+ \rightarrow H^+ + CH_3COH \quad (5)$$

$$2H^+ + 2e^- \rightarrow H_2 \quad (6)$$

$$H^+ + AB \rightarrow C_6H_5NH_2\ (\text{aniline}) \quad (7)$$

$$H^+ + MO \rightarrow C_6H_6NNaO_3S\ (\text{sodium sulfanilate}) + (CH_3)_2NC_6H_4NH_2\ (\text{p-aminodimethylaniline}) \quad (8)$$

■■Dear author please mention Figure 11■■The photocatalytic mechanism was schematically depicted in Figure 10, in which the bandgap position of 2% Ni CdS catalyst was determined with DRS and Mott Schottky measurements. Under visible light illumination, Ni-CdS catalyst generated H^+ ions, which were adsorbed on catalyst surfaces and ready for hydrogenation reaction to cleave azo bonds of AB and MO in aqueous solution. Photocatalytic HER and hydrogenation reaction to cleave azo bonds were competitive with each other. The lifetime of H^+ ions should be sufficient for hydrogenation reaction; otherwise, they would be reduced by the photo-generated electron to form hydrogen gases.

3. Conclusions

Ni-doped CdS photocatalysts had been synthesized with different amounts of Ni dopant. It was identified that the XRD patterns were shifted to a higher angle to indicate the incorporation of Ni into CdS lattice. Based on the TPC and EIS analyses, incorporating 2% Ni significantly induced a better photoresponse and lower the charge transfer resistivity. However, with higher percentages of Ni dopant, a little precipitation of Ni metal degraded the performance of catalyst. Based on the proofs that the decreasing peak at 320 nm for cis-AB and at 462 nm for MO and the emergences of new peaks at 239 nm for aniline and at 244 nm for the products of MO reduction, the photocatalytic reactions had successfully cleaved the azo bonds in AB and MO compounds in the presences of Ni-CdS catalysts. The reusability experiments and CV measurement also indicated the stability of catalyst for long term application. This work contributed not only to a strategy to improve the HER rate but also to improve the utilization of catalyst for chemical conversion in a mild condition.

Supporting Information Summary

Supporting information contains experimental procedures, including materials used in this work, synthesis and characterization methods, photocatalytic experimental procedures, and ICP analysis.

Acknowledgments

Authors thank the Department of Chemistry, Universitas Sumatera Utara that provided the facilities to conduct all the analyses and experiments.

Conflict of Interest

The authors declare no conflict of interest.

Keywords: alloys · azo bonds · hydrogenation · Ni-CdS · photocatalysis · radicals · visible light

[1] a) W. L. Kebede, D.-H. Kuo, F. T. Bekena, L. W. Duresa, *Chemosphere* **2020**, *254*, 126823; b) Y. Shiraishi, M. Katayama, M. Hashimoto, T. Hirai, *Chem. Commun.* **2018**, *54*, 452–455; c) J.-A. Quek, S.-M. Lam, J.-C. Sin, A. R. Mohamed, *J. Photochem. Photobiol. B* **2018**, *187*, 66–75; d) S. Li, G. Dong, R. Hailili, L. Yang, Y. Li, F. Wang, Y. Zeng, C. Wang, *Appl. Catal. B* **2016**, *190*, 26–35; e) H. Abdullah, D.-H. Kuo, J.-Y. Lee, C.-M. Wu, *Appl. Phys. A* **2016**, *122*, 750; f) H. Abdullah, D.-H. Kuo, Y.-R. Kuo, F.-A. Yu, K.-B. Cheng, *J. Phys. Chem. C* **2016**, *120*, 7144–7154; g) H. Abdullah, D.-H. Kuo, *Appl. Phys. A* **2016**, *122*, 739; h) H. Abdullah, D.-H. Kuo, *ACS Appl. Mater. Interfaces* **2015**, *7*, 26941–26951; i) M. M. Mohamed, M. S. Al-Sharif, *Appl. Catal. B* **2013**, *142–143*, 432–441; j) T. T. Le, M. S. Akhtar, D. M. Park, J. C. Lee, O. B. Yang, *Appl. Catal. B* **2012**, *111*, 397–401.

[2] M. M. Khan, D. Pradhan, Y. Sohn, *Nanocomposites for Visible Light-induced Photocatalysis*, Springer International Publishing, **2017**, 101.

[3] a) H. Jiang, Y. Lin, B. Chen, Y. Zhang, H. Liu, X. Duan, D. Chen, L. Song, *Mater. Today* **2018**, *21*, 602–610; b) M. Ye, X. Gao, X. Hong, Q. Liu, C. He, X. Liu, C. Lin, *Sustain. Energy Fuels* **2017**; c) S. Nanda, R. Rana, Y. Zheng, J. A. Kozinski, A. K. Dalai, *Sustain. Energy Fuels* **2017**; d) C. Marchal, A. Piquet, M. Behr, T. Cottineau, V. Papaefthimiou, V. Keller, V. Caps, *J. Catal.* **2017**, *352*, 22–34; e) L. Pan, S. Wang, J. Xie, L. Wang, X. Zhang, J.-J. Zou, *Nano Energy* **2016**, *28*, 296–303; f) N. S. Gultom, H. Abdullah, D.-H. Kuo, *Appl. Catal. B* **2020**, *272*, 118985; g) H. Abdullah, N. S. Gultom, D.-H. Kuo, *Appl. Catal. B* **2020**, *261*, 118223; h) H. Abdullah, N. S. Gultom, D.-H. Kuo, A. D. Saragih, *New J. Chem.* **2018**.

[4] a) H. Abdullah, Y.-R. Ko, D.-H. Kuo, N. S. Gultom, *ACS Appl. Mater. Interfaces* **2020**, *12*, 16186–16199; b) O. A. Zelekew, D.-H. Kuo, H. Abdullah, *Adv. Powder Technol.* **2019**, *30*, 3099–3106; c) F. T. Bekena, H. Abdullah, D.-H. Kuo, M. A. Zeleke, *J. Ind. Eng. Chem.* **2019**, *78*, 116–124; d) H. Abdullah, D.-H. Kuo, N. S. Gultom, *Catal. Sci. Technol.* **2019**.

[5] H. Tada, T. Ishida, A. Takao, S. Ito, *Langmuir* **2004**, *20*, 7898–7900.

[6] a) N. S. Gultom, H. Abdullah, D.-H. Kuo, *J. Phys. Conf. Ser.* **2018**, *1007*, 012061; b) F. Mahdavi, T. C. Bruton, Y. Li, *J. Org. Chem.* **1993**, *58*, 744–746.

[7] a) H. Abdullah, N. S. Gultom, D.-H. Kuo, *New J. Chem.* **2017**, *41*, 12397–12406; b) H. Abdullah, D.-H. Kuo, X. Chen, *Int. J. Hydrogen Energy* **2017**,

42, 5638–5648; c) N. S. Gultom, H. Abdullah, D.-H. Kuo, *Int. J. Hydrogen Energy* **2017**, *42*, 25891–25902; d) N. S. Gultom, H. Abdullah, D.-H. Kuo, *J. Energy Inst*. **2019**, *92*, 1428–1439.

[8] a) A.-M. Alexander, J. S. J. Hargreaves, *Chem. Soc. Rev*. **2010**, *39*, 4388–4401; b) C. Avelino, C. Patricia, S. Pedro, *Angew. Chem. Int. Ed.* **2007**, *46*, 7266–7269; *Angew. Chem.* **2007**, *119*, 7404–7407; c) M. Boronat, P. Concepción, A. Corma, S. González, F. Illas, P. Serna, *J. Am. Chem. Soc.* **2007**, *129*, 16230–16237; d) A. Corma, P. Serna, P. Concepción, J. J. Calvino, *J. Am. Chem. Soc.* **2008**, *130*, 8748–8753; e) A. Corma, P. Serna, *Sci. J.* **2006**, *313*, 332–334.

[9] B. Saha, S. De, S. Dutta, *Crit. Rev. Environ. Sci. Technol.* **2013**, *43*, 84–120.

[10] a) J. Wang, Z. Yuan, R. Nie, Z. Hou, X. Zheng, *Ind. Eng. Chem. Res.* **2010**, *49*, 4664–4669; b) H. Li, Q. Zhao, Y. Wan, W. Dai, M. Qiao, *J. Catal.* **2006**, *244*, 251–254; c) S.-P. Lee, Y.-W. Chen, *J. Mol. Catal. A* **2000**, *152*, 213–223.

[11] H.-Y. Jiang, J. Xu, B. Sun, *Appl. Organomet. Chem.* **2018**, *32*, e4260.

[12] N. Daems, J. Wouters, C. Van Goethem, K. Baert, C. Poleunis, A. Delcorte, A. Hubin, I. F. J. Vankelecom, P. P. Pescarmona, *Appl. Catal. B* **2018**, *226*, 509–522.

[13] G. Xiao, P. Li, Y. Zhao, S. Xu, H. Su, *Chem. Asian J.* **2018**, *13*, 1950–1955.

[14] J. Liu, N. Ma, W. Wu, Q. He, *Chem. Eng. J.* **2020**, 124719.

[15] a) A. L. Luna, D. Dragoe, K. Wang, P. Beaunier, E. K. Kowalska, B. Ohtani, D. Bahena Uribe, M. A. Valenzuela, H. Remita, C. Colbeau-Justin, *J. Phys. Chem. C* **2017**; b) T. Aditya, J. Jana, N. K. Singh, A. Pal, T. Pal, *ACS Omega* **2017**, *2*, 1968–1984; c) O. Ahmed Zelekew, D.-H. Kuo, *Phys. Chem. Chem. Phys.* **2016**, *18*, 4405–4414; d) Y. Wang, L. Liu, L. Xu, X. Cao, X. Li, Y. Huang, C. Meng, Z. Wang, W. Zhu, *Nanoscale* **2014**, *6*, 6790–6797; e) J. Jitputti, Y. Suzuki, S. Yoshikawa, *Catal. Commun.* **2008**, *9*, 1265–1271.

[16] S. Hejazi, M. Altomare, N. T. Nguyen, S. Mohajernia, M. Licklederer, P. Schmuki, *Appl. Mater. Res.* **2019**, *14*, 118–125.

[17] H. Abdullah, D.-H. Kuo, *Int. J. Hydrogen Energy* **2019**, *44*, 191–201.

[18] a) Q. Li, B. Guo, J. Yu, J. Ran, B. Zhang, H. Yan, J. R. Gong, *J. Am. Chem. Soc.* **2011**, *133*, 10878–10884; b) T. Zuo, Z. Sun, Y. Zhao, X. Jiang, X. Gao, *J. Am. Chem. Soc.* **2010**, *132*, 6618–6619.

[19] a) K. Wu, Z. Chen, H. Lv, H. Zhu, C. L. Hill, T. Lian, *J. Am. Chem. Soc.* **2014**, *136*, 7708–7716; b) M. D. Regulacio, C. Ye, S. H. Lim, M. Bosman, L. Polavarapu, W. L. Koh, J. Zhang, Q.-H. Xu, M.-Y. Han, *J. Am. Chem. Soc.* **2011**, *133*, 2052–2055.

[20] a) I. S. Yahia, I. M. El Radaf, A. M. Salem, G. B. Sakr, *J. Alloys Compd.* **2019**, *776*, 1056–1062; b) A. Rmili, F. Ouachtari, A. Bouaoud, A. Louardi, T. Chtouki, B. Elidrissi, H. Erguig, *J J. Alloys Compd.* **2013**, *557*, 53–59.

[21] A. Kumar, R. K. Sharma, N. Goyal, S. Gautam, *Vacuum* **2019**, *160*, 75–80.

[22] A. Firdous, D. Singh, M. M. Ahmad, *Appl. Nanosci.* **2013**, *3*, 13–18.

[23] J. C. Slater, *J. Chem. Phys.* **1964**, *41*, 3199–3204.

[24] X. Chen, W. Shangguan, *Front. Energy* **2013**, *7*, 111–118.

[25] a) L. Gomathi Devi, S. Girish Kumar, K. Mohan Reddy, C. Munikrishnappa, *J. Hazard. Mater.* **2009**, *164*, 459–467; b) L.-Q. Zheng, X.-D. Yu, J.-J. Xu, H.-Y. Chen, *Chem. Commun.* **2015**, *51*, 1050–1053.

[26] H. Shuwanto, N. S. Gultom, H. Abdullah, D.-H. Kuo, *ACS Appl. Mater. Interfaces* **2020**, *3*, 12692–12702.

Submitted: November 9, 2020
Accepted: February 18, 2021

FULL PAPERS

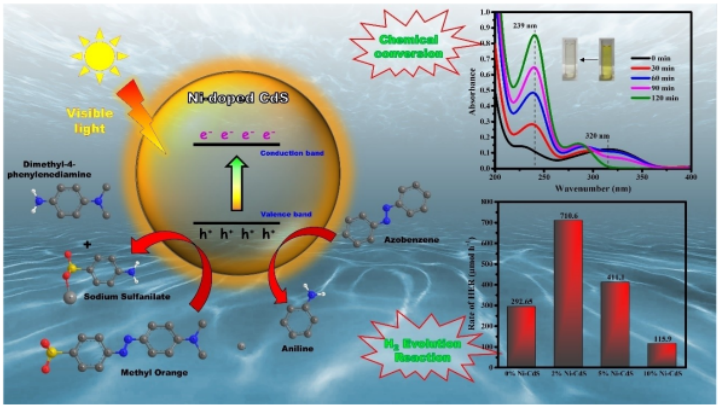

Dr. H. Abdullah, Dr. R. Siburian, Dr. S. P. Pasaribu, Prof. A. S. Pangga-bean*

1 – 11

Visible-Light Driven Ni-Incorpo-rated CdS Photocatalytic Activities for Azo-Bond Cleavages with Hy-drogenation Reaction

The catalytic performances of 2% Ni-CdS exhibited excellent electrical and photoresponse properties. It has been demonstrated the possibility of indus-trial application with Ni-CdS catalyst. The catalyst can achieve a hydrogen evolution rate of ~710 μmol/h and the evolved hydrogen can be used for hydrogenation reaction to cleave azo-bonds in MO and azobenzene. Ni-CdS catalyst's reusability has been shown for several runs and is further examined with cyclic voltammetry for 100 cycles without any significant degradation.

Hairus_Abdullah_et_al._Chemistry_Select_2021.pdf

ORIGINALITY REPORT

17%	10%	14%	2%
SIMILARITY INDEX	INTERNET SOURCES	PUBLICATIONS	STUDENT PAPERS

MATCH ALL SOURCES (ONLY SELECTED SOURCE PRINTED)

6%

★ pubs.rsc.org

Internet Source

Exclude quotes	Off	Exclude matches	Off
Exclude bibliography	On		